A Small Oxazine Compound as an Anti-Tumor Agent: A Novel Pyranoside Mimetic That Binds to TNF-α, HB-EGF and VEGF

Basappa[1,2,8,9], Akiko Saito[3], Sengottuvelan Murugan[1,9], Chandagirikoppal V. Kavitha[4], Kottayath G. Nevin[1], Kazuki N. Sugahara[5,6], Yasumitsu Kondoh[3], Chun Man Lee[7], Masayuki Miyasaka[5], Hiroyuki Osada[3], Kanchugarakoppal S. Rangappa*[4], and Kazuyuki Sugahara*[1,2]

[1]Faculty of Advanced Life Sciences, Hokkaido University, Sapporo, Japan, [2]Department of Biochemistry, Kobe Pharmaceutical University, Kobe, Japan, [3]Antibiotics Laboratory, Chemical Biology Department, Advanced Science Institute, RIKEN, Japan, [4]Department of Studies in Chemistry, University of Mysore, Mysore, India, [5]Laboratory of Immunodynamics, Department of Microbiology and Immunology, Osaka University of Graduate School of Medicine, Suita, Japan, [6]Vascular Mapping Centre, Burnham Institute for Medical Research, UCSB, University of CA, Santa Barbara, USA, [7]Medical Centre for Translational Research, Osaka University Hospital, Suita, Japan, [8]Department of Chemistry, Bangalore University, Bangalore, India.

Running Title: Anti-tumor activity of a pyranoside mimetic.

Key Words: Pyranoside mimetic, Anti-tumor, Metastasis, Growth factor, Heparanase

Note: [9]Supported by a postdoctoral fellowship from the Japan Society for the Promotion of Science (JSPS).
Supplementary data for this article are available at Cancer Research Online.

***Corresponding authors**

Address correspondence to Kanchugarakoppal S. Rangappa, Department of Studies in Chemistry, University of Mysore, Manasagangotri, Mysore-570 006, India. Tel/Fax: +91-821-2412191; E-mail: rangappaks@yahoo.com

Address correspondence to Kazuyuki Sugahara, Laboratory of Proteoglycan Signaling and Therapeutics, Graduate School of Life Sciences, Hokkaido University, Frontier Research Centre for Post-Genomic Science and Technology, Nishi 11, Kita 21, Kita-ku, Sapporo, Hokkaido 001-0021, Japan. Tel: 81-(11)-706-9054; Fax: 81-(11)-706-9056; E-mail: k-sugar@sci.hokudai.ac.jp.

Abstract

A novel pyranoside mimetic compound, DMBO (2-(2,6-difluorophenyl)-4a,5,6,7,8,8a-hexahydro-4a-(4-methoxyphenyl)-4*H*-benzo[e][1,3]oxazine), was designed and synthesized. The sugar mimicking behavior of DMBO was addressed by its ability to bind several cytokines/growth factors such as tumor necrosis factor (TNF)-α, heparin-binding epidermal growth factor-like growth factor (HB-EGF) and vascular endothelial growth factor (VEGF) involved in cancer progression as detected through novel surface plasmon resonance imaging. In addition, DMBO inhibited the binding of TNF-α to anti-TNF-α antibody *in vitro* and also the production of TNF-α *in vivo*. The effect of DMBO on TNF-α was supported by our finding that it inhibited the proliferation of metastatic human ovarian cancer cell line (OVSAHO), which abundantly express TNF-α. High-throughput screening of DMBO showed a significant inhibition of heparanase activity at higher concentrations *in vitro*. DMBO also affected the heparan-degrading activity of mouse osteosarcoma cell line (LM8G7) in a dose-dependent manner, and showed a prominent inhibitory effect on the metastasis of LM8G7 cells to mouse liver. These responses are associated with the strong inhibition of migration, adhesion, invasion and proliferation of LM8G7 cells and also with the anti-angiogenic activity of DMBO. In addition, DMBO markedly inhibited the ectopic secretion of VEGF by LM8G7 cells, which drives the metastatic potential of LM8G7. Furthermore, the interaction of DMBO with HB-EGF was significantly correlated with inhibition of the proliferation of human ovarian cancer cell line (SKOV-3). These results emphasize that DMBO mimics heparan sulfate structurally and its anti-metastatic activity is likely expressed through binding to multiple factors, which are critical for tumor development and progression.

Introduction

Synthetic heterocyclic compounds have been used extensively for drug development and the treatment of diseases including cancer (1). Among them, oxazines are well known for their potential biological effects, for example, the inactivation of chymotrypsin by 5-butyl-3*H*-l,3-oxazine-2,6-dione (2). In addition, 5-β-D-ribofuranosyl-l,3-oxazin-2,4-dione, a C-ribonucleoside antibiotic (minimycin), is used as an anti-tumor agent (3) and 5-methyl-3*H*-1,3-oxazine-2,6-dione is used as a suicide inactivator of serine proteases (4). In the search for an effective therapeutic agent for cancer, which targets multiple pathways, we designed and synthesized a novel six-membered oxazine compound, DMBO (2-(2,6-difluorophenyl)-4a,5,6,7,8,8a-hexahydro-4a-(4-methoxyphenyl)-4*H*-benzo[e][1,3]oxazine), a class of sugar mimetic, in which the ring carbon has been replaced by a nitrogen atom. DMBO is considered to mimic the pyranoside structure of sugar residues in heparan sulfate (HS).

HS on cell surfaces modulates signal transduction to tumor cells by interacting with various growth factors such as fibroblast growth factor-2 (FGF-2) (5), vascular epidermal growth factor (VEGF) (6), and heparin-binding epidermal growth factor-like growth factor (HB-EGF) (7). Cell surface and extracellular matrix HS plays a major role in tumor metastasis, and acts as a storage shed for various proteins (8). Heparanase, an endo-β-D-glucuronidase family member, promotes tumor cell invasion by degrading HS in the extracellular matrix (ECM) (9, 10). Heparanase promotes cell proliferation, metastasis and angiogenesis by releasing growth factors such as FGF-2 and VEGF from HS (11, 12). Several studies have shown that HS mimetics act as antitumor agents. For example, anti-tumor and anti-heparanase activities of a non-sugar-based HS mimetic compound KI-105 have been reported (13).

In addition to the matrix components and matrix-degrading enzymes, malignant cells produce a variety of soluble factors such as tumor necrosis factor-α (TNF-α), VEGF, and

HB-EGF, which play a major role in tumor progression. Heparin-binding growth factors like FGF-2, VEGF and HB-EGF have been implicated in the metastatic process (14). Increasing evidence shows that TNF-α acts as a key mediator for local inflammation and also in the development of cancer, suggesting that anti-TNF-α therapy might be effective against pancreatic tumor growth and metastasis (15). VEGF plays a major role in both vasculogenesis and angiogenesis by triggering a tyrosine kinase pathway (16). Some members of the VEGF family stimulate cellular responses by binding to cell-surface HS-PGs as co-receptors (17). Therefore, effective VEGF antagonists or the VEGF receptor agonists that mimic HS may be good tools to inhibit VEGF production. HB-EGF activates at least three signal transduction pathways, which are involved in proliferation, the secretion of VEGF, and the stimulation of chemotaxis in cancer cells (18). The expression of ligands for the EGF receptor (EGFR), such as transforming growth factor-α, is also often increased in gliomas, resulting in an autocrine loop that contributes to the growth autonomy of glioma cells (19). Importantly, HB-EGF and EGF act downstream by binding to EGFR on the cell surface with high affinity (20). Therefore, it is reasonable to expect either inhibition of the expression of HB-EGF or blocking of the EGFR pathway to have therapeutic value in the treatment of a variety of cancers. This notion is consistent with the finding that a neutralizing antibody against HB-EGF blocked the transactivation of EGFR and inhibited cell proliferation (21).

DMBO mimics HS structurally. Here, we demonstrate DMBO's ability to bind various growth factors/cytokines such as TNF-α, VEGF and HB-EGF, anti-inflammatory activity, and anti-metastatic activity *in vivo*.

Materials and Methods

Chemicals. Cisplatin, suramin, recombinant human HB-EGF (rh-HB-EGF), rh-midkine, rh-TNF-α, rh-FGF-2, rh-$VEGF_{165}$, and rh-pleotrophin were purchased from Wako Pure Chemicals Co. (Osaka, Japan). Mifepristone and lipopolysaccharide (LPS) were from Sigma (St. Louis, MO). 100X non-essential amino acids, β-mercaptoethanol, 100X sodium pyruvate and L-glutamine were from GIBCO (Auckland, New Zealand). The cell proliferation assay kit Tetracolor One was obtained from Seikagaku Corp. (Tokyo, Japan) and the Diff-Quick solution was from International Reagent Corp. (Kobe, Japan). All other chemicals and reagents used were of the highest commercial grade available. The synthesis, characterization and the crystal structure of DMBO used in this study are described in the Supplementary Information.

Animals and cell lines. Nine-week-old female C3H/HeN mice and 10-week-old male C57BL/6 mice were obtained from Japan SLC (Hamamatsu, Japan) and kept in standard housing. All the experiments were performed according to a protocol approved by the local animal care committee of Hokkaido University. LM8G7, a highly metastatic murine osteosarcoma cell line with the potential to invade the liver, was cloned from LM8G5 cells (22) as described (23) and cultured in Dulbecco's Modified Eagle's Medium (DMEM) supplemented with 10% (v/v) fetal bovine serum (FBS) (Thermo Trace, Melbourne, Australia), streptomycin (100 μg/ml), penicillin (100 units/ml), 100X non-essential amino acids, β-mercaptoethanol (50 μM), 100X sodium pyruvate, and L-glutamine (2 mM) at 37 °C in a humidified 5% CO_2 atmosphere. The cells were harvested after incubation with 0.1% trypsin/1 mM EDTA in PBS for 5 min at 37 °C followed by gentle flushing with a pipette, and subcultured thrice a week. Human ovarian cancer cells (OVSAHO and SKOV-3) and mouse vascular endothelial cells (UV♀2) were purchased from RIKEN Cell Bank, Japan. The OVSAHO cells were cultured in RPMI medium supplemented with 10% (v/v) FBS, L-

glutamine (2 mM), and $NaHCO_3$ (10%). The SKOV-3 cells were cultured in McCoy's 5A medium supplemented with 10% (v/v) FBS and L-glutamine (2 mM). The UV♀2 cells were maintained in DMEM supplemented with 10% (v/v) FBS.

Surface plasmon resonance (SPR) assay. To introduce DMBO onto a gold surface for SPR measurements, photoaffinity-linker-coated gold substrates (PGSs) were prepared according to our previous report (24). The detailed materials and methods for the SPR assay are provided in Supplementary Information. The interaction between DMBO and the growth factors/cytokines such as TNF-α, HB-EGF, and VEGF were carried out using SPR imaging instrument (TOYOBO, Osaka, Japan). The SPR image and signal data were collected with an SPR analysis program (TOYOBO). The SPR difference image was constructed by using the Scion Image program (Scion, MD).

TNF-α binding assay. The binding of TNF-α to its antibody was measured using a colorimetric-based Quantikine ELISA kit (R&D systems). The effects of DMBO on the binding were determined by incubating different concentrations of DMBO (15 to 148 μM) with the recombinant mouse TNF-α for 30 min at room temperature, transferring 100 μL of the reaction mixture to a 96-well plate coated with a polyclonal antibody specific for mouse TNF-α, incubating for 2 h at room temperature. After washing, 100 μL of horseradish peroxidase (HRP)-conjugated anti-TNF-α antibody was added to each well. The mixture was incubated for another 2 h, aspirated, washed and mixed with 100 μL of the substrate solution (a mixture of H_2O_2 and tetramethyl benzidine). After 30 min at room temperature, 100 μL of a stop solution (dil. HCl) was added and the optical density was determined using a model 680 micro plate reader (Bio-Rad) at 450 nm. Heparin (50 μg/ml) from porcine intestinal mucosa was used as a positive control.

Anti-inflammatory assay. C57BL/6 mice (20-25g) were injected intraperitoneally with 2 ml of 3% thioglycolate (TG) broth (Sigma-Aldrich) or sterile-saline as described

earlier (25). After 10 min, DMBO (0.5, 1.5 or 5 mg/kg) suspended in saline was injected through a lateral tail vein. After 24 h, LPS (1.0 μg) was injected intraperitoneally, and 1 h later, the peritoneal cavities were lavaged with 4 ml of PBS containing 3 mM EDTA. After the total number of inflammatory cells was counted, the lavage fluid (2 ml) was centrifuged at 1,500 rpm for 5 min, and the supernatant was stored at -20 °C for the detection of TNF-α. The amount of TNF-α was determined by using a Quantikine ELISA kit. Heparin (10 mg/kg) was used as a positive control.

Liver metastasis assay. C3H/HeN mice were intravenously injected with 1 x 10^6 LM8G7 cells in 200 μL of DMEM via the tail. Some mice received an intravenous injection of DMBO (0.5, 1.0 or 1.5 mg/kg) suspended in 200 μL of DMEM, 30 min prior to the tumor cell injection. After 4 weeks, the mice were sacrificed, the number of liver nodules was counted macroscopically, and liver weight was measured in the control and DMBO-treated animals. Heparin (5 mg/kg) was used as a positive control.

Wound healing assay. LM8G7 cells were seeded in a 6-well plate and allowed to grow to complete confluence. Subsequently, a plastic pipette tip was used to scratch the cell monolayer to create a cleared area, and the wounded LM8G7 cell layer was washed with a fresh medium to remove loose cells, and photographed using CKX41 Olympus microscope (Olympus, Tokyo, Japan) equipped with x10 objective lenses. The cells were incubated with or without DMBO (0.2 μM), and the inhibition of the wound healing by DMBO was measured after 24 h incubation. The percentage of the distance of the DMBO-treated area compared with that of the control wound area was calculated.

Cell adhesion assay. Tumor cell adhesion to immobilized P-selectin or fibronectin was quantitated as described previously (26, 27). Briefly, a 96-well microtiter plate (Maxisorp; Nunc, Roskilde, Denmark) was coated with P-selectin (5 μg/ml in PBS) or fibronectin (5 μg/ml in 0.1 M $NaHCO_3$) at 4 °C overnight. The plate was washed three times

with PBS, blocked with 3% bovine serum albumin (BSA) in PBS for 2 h at room temperature, and washed again. The plate was incubated with DMBO (27 or 54 μM) in 100 μl of DMEM for 1 h at room temperature, and rinsed three times with DMEM. LM8G7 (2 x 10^4) cells in 100 μl of DMEM were added to each well and incubated for 1 h at 37 °C. Non-adherent cells were removed by washing thrice with DMEM. The adhered cells were quantified by adding 5 μL of TetraColor One, and the mixture was incubated for an additional 4 h (28). Absorbance at 450 nm was monitored to quantify the adhered cells. % inhibition of the adhered cells by DMBO was calculated by comparing with the control cells.

***In vitro* invasion assay.** The invasion of LM8G7 cells across Matrigel^{TM}-coated porous membranes was assessed using 24-well plates (8 μm pore size, insert size: 6.4 μm) (BD Biosciences) according to the manufacturer's protocol. Briefly, single cell suspensions of LM8G7 (6 x 10^4 cells/ml) were prepared by detaching and resuspending the cells in DMEM containing 0.1% BSA. Before the cells were added, the chambers were rehydrated for 2 h in an incubator at 37 °C. The lower chambers were filled with DMEM containing 0.1% BSA and 5% FBS. After the addition of the cells with or without DMBO (0.2 or 0.5 μM) to the upper chamber, the Matrigel^{TM} invasion chambers were incubated for a further 22 h at 37 °C. The cells that had not invaded were removed from the upper surface of the membrane by scrubbing. The cells that had invaded through the filter were fixed and stained with a Diff Quick solution.

***In vitro* cell proliferation assay.** UV♀2 or SKOV-3 cells were seeded at a density of 1 x 10^3 cells/well in a 96-well plate and incubated overnight at 37 °C. The cells were treated with predetermined concentrations of DMBO for an additional 48 h. The DMSO solution of DMBO was diluted with DMEM (150 μL) to yield a final concentration of 195 μM (final concentration of DMSO, < 0.1%). The viability of control cells and cells treated with DMBO

was measured using TetraColor One. Absorbance at 450 nm was monitored to calculate the viability of the cells in percentage terms.

Real-time proliferation assay. The cell proliferation assay was done using the Real-Time Cell Electronic Sensing (RT-CES) system (ACEA Biosciences, San Diego, CA). OVSAHO (15 x 10^3 cells/well) or LM8G7 (5 x 10^3 cells/well) cells were seeded in ACEA's 96X e-plate™ in a final volume of 150 μL (29). Approximately 24 h after seeding, when in a log growth phase, the cells were incubated with 150 μL of DMEM containing various concentrations of DMBO (24 to 197 μM) or DMEM containing DMSO as a control. The effects of DMBO on the proliferation of OVSAHO or LM8G7 cells were monitored dynamically every 10 min. A cell index (quantitative measurement of cell proliferation) was plotted against time. The IC_{50} values were calculated from concentration-response curves by a non-linear regression analysis using the GraphPad Prism (GraphPad Prism Software Inc., San Diego).

***In vitro* angiogenesis assay**. *In vitro* angiogenesis assay was performed according to the previously reported procedure (30). Details are provided in Supplementary Information.

Heparanse activity assay. A heparan-degrading assay kit (Takara Biomedical, Otsu, Japan) was used according to the manufacturer's directions. Briefly, 50 μL of biotinylated HS was incubated with 31 mIU of recombinant human heparanase in the presence or absence of serially diluted DMBO (59 to 236 μM). After 45 min at 37 °C, the reaction mixture was transferred to a microplate, where a fusion protein comprising the cell binding domain of human fibronectin and human FGF-2 was immobilized, and incubated at 37 °C for 15 min. The wells were washed, 100 μL of an avidin-peroxidase (POD) conjugate and 100 μL of POD substrate were added, and the mixture was incubated for 30 min. The reaction was stopped by adding 100 μL of a stop solution and the absorbance was measured at 450 nm. Suramin (70 μM) was used as a positive control (31).

***In vitro* heparan-degrading assay.** LM8G7 (1 x 10^6) cells were seeded into a 6-well plate and incubated overnight. After 24 h, the cells were incubated with DMBO at concentrations of 55, 104, and 206 μM in triplicate. To determine the effect of DMBO on the heparan-degrading activity of LM8G7, the cells were further incubated for 48 h at 37 °C. The cells were collected by centrifugation, and a whole-cell lysate was prepared as reported (32). Protein concentrations of the samples were determined using a BCA (bicinchoninic acid) assay kit (Thermo Fisher Scientific Inc., IL), and adjusted to 0.1 mg/ml. The heparan-degrading activity in DMBO-treated/untreated cell lysates was measured.

VEGF quantification assay. LM8G7 (1 x 10^6) cells were seeded into a 6-well plate and incubated overnight. After 24 h, the medium was replaced with a fresh serum-free medium containing 74, 148, or 295 μM of DMBO to analyze the effects of DMBO on VEGF's secretion. The cells were further incubated for 48 h at 37 °C. The medium was collected and centrifuged at 5,000 rpm for 5 min at 4 °C, and the protein concentration was determined. The quantification of mouse VEGF was done using the Quantikine Immunoassay Kit (R&D systems). Briefly, with known amounts of recombinant VEGF as standards, the control or DMBO-treated cell lysates were added to a 96-well plate, which was pre-coated with the polyclonal antibody specific to mouse VEGF, and incubated for 2 h. Bound VEGF was detected by adding an HRP-conjugated polyclonal antibody against mouse VEGF. After 2 h, 100 μL of the substrate chromogen was added and allowed to react for 30 min with the POD-conjugate. The reaction was stopped and the VEGF content was quantified in a micro-plate reader at 450 nm.

Statistical analysis. The statistical analysis was done using a software Origin 8 (OriginLab). The Mann-Whitney *U* test was used to determine P-values.

Results

Synthesis of DMBO. The DMBO was prepared by the cyclization of 1-[2-amino-1-(4-methoxy-phenyl)-ethyl]-cyclohexanol monoacetate with 2,6-difluoro benzaldehyde in the presence of potassium carbonate (Supplementary Fig. S1A). Further, we obtained DMBO in single crystalline form (Supplementary Fig. S1B). The comparison of the pyranose ring of the HS disaccharide unit and its mimetic oxazine ring of DMBO is also provided (Supplementary Fig. S1C).

Examination of the binding of DMBO to growth factors and chemokines. In recent years, many high-throughput methodologies have been developed to identify potential anti-cancer molecules. We conducted a novel SPR assay to screen the ability of small molecules to bind various cytokines/growth factors such as TNF-α, HB-EGF and VEGF. Recently, we improved our photoaffinity SPR imaging technique by reviewing the thiol linkers used to coat the surface of the gold substrate. A new photoaffinity linker (Supplementary Fig. S2) improved the sensitivity with which the interaction between small molecules and proteins was detected, and allowed the detection of the direct binding of cytokines/growth factors to small molecules. An overview of the SPR analysis is shown in Fig. 1A. DMBO and other screened small molecules were immobilized on the PGSs. In our *in vitro* experimental conditions, strong SPR signals for the direct binding of DMBO with TNF-α, HB-EGF, and VEGF were found (Fig. 1B-D; Supplementary Fig. S3-S5).

Inhibition by DMBO of the binding of TNF-α to anti-TNF-α antibody. TNF-α is a key factor in inflammation and the progression of cancer. To determine whether DMBO, a sugar mimicking molecule, can block the binding of TNF-α to its antibody, DMBO was incubated *in vitro* with recombinant TNF-α, and its inhibitory effect was quantified. DMBO dose-dependently (15 to 148 μM) inhibited the binding of TNF-α to its antibody (Fig. 2A).

Effects of DMBO on the secretion of TNF-α *in vivo*. Further, the effects of DMBO on the local production of TNF-α in the peritoneal cavities of TG-treated mice were

examined to confirm the anti-inflammatory role of DMBO. DMBO effectively inhibited the infiltration of inflammatory cells in the lavage fluid by 47, 55, and 64% at 0.5, 1.5, and 5 mg/kg, respectively, as compared to the control (Fig. 2B). Heparin (10 mg/kg), as a positive control, inhibited the infiltration of inflammatory cells in the lavage fluid by 81%. In addition, higher levels of TNF-α were detected in the mice primed with TG and LPS, compared to saline-injected control mice. TNF-α release was reduced from 42 (control) to 26, 22, or 19 x 10^{-2} ng/ml, corresponding to 38, 46, and 55% reduction as compared to control at 0.5, 1.5, and 5 mg/kg of DMBO, respectively (Fig. 2C). Heparin, a positive control, inhibited TNF-α release from 42 to 12 x 10^{-2} ng/ml, corresponding to 70% reduction at 10 mg/kg dose.

DMBO prevents liver metastasis *in vivo*. Inhibition of metastasis represents an attractive approach to the treatment of highly malignant tumors. Mice given an intravenous injection of LM8G7 cells developed copious metastatic nodules in the liver within 30 days (Fig. 3A). In contrast, mice treated intravenously with DMBO at 0.5, 1.0 or 1.5 mg/kg were completely free of metastatic nodules in the liver (Fig. 3B). Measurements of liver weight, which reflects tumor burden, gave similar results, with DMBO almost completely suppressing the increase in liver weight by inhibiting the formation of tumor nodules. The animals tolerated the dosages of DMBO well, showing no signs of toxicity or weight loss during the experiments. Heparin (5 mg/kg), a positive control, also prevented the increase in liver weight (Fig. 3C) by suppressing the formation of metastatic nodules in the liver.

Effects of DMBO on the migration, adhesion and invasion of LM8G7 cells. Effects of DMBO on the migration, adhesion and invasion of highly metastatic LM8G7 cells were studied. The wound healing assay was performed to examine its effects on migration. DMBO (0.2 μM) completely inhibited the migration of LM8G7 cells after a scratch was made (Fig. 4A). The distance between the edges of the wound was measured at 0 h and

normalized to 100% (Fig. 4B). We next examined the effect of DMBO (27 or 54 μM) on the adhesion of LM8G7 cells to P-selectin or fibronectin. DMBO inhibited the adhesion LM8G7 cells to P-selectin by 36 and 48% (Fig. 4C) as compared to control, which is relatively weaker when compared to the inhibition of the adhesion to fibronectin by 48 and 72% at 27 and 54 μM, respectively. Further, DMBO inhibited the invasion of LM8G7 cells into Matrigel^{TM} at 0.2 and 0.5 μM by 74 and 75%, respectively, as compared to the control (Fig. 4D).

Effects of DMBO on the viability and proliferation of normal and cancer cells. Given the importance of DMBO as an anti-inflammatory and anti-metastatic agent, its effects on the proliferation of various tumor cells were examined. First, however, the cytotoxicity of DMBO was tested using mouse endothelial cells (UV♀2). DMBO had no significant effect on the proliferation of UV♀2 cells (13% inhibition at 195 μM), whereas mifepristone (33) strongly inhibited proliferation (87% at 155 μM) (Fig. 5A). However, DMBO inhibited the proliferation of HB-EGF-positive SKOV-3 cells dose-dependently. DMBO at 195 μM completely inhibited the proliferation of SKOV-3 cells (99%), whereas mifepristone at 155 μM had a lesser effect (63%) (Fig. 5B). Further, the effects of DMBO (24 to 197 μM) on the proliferation of OVSAHO and mouse osteosarcoma LM8G7 cells were monitored using the RT-CES system. DMBO inhibited the proliferation of highly metastatic TNF-α-expressing OVSAHO and VEGF-expressing LM8G7 cells dose-dependently (Fig. 5C & D) with an IC_{50} value of 6 and 13 μM, respectively. Therefore, the above results indicated that DMBO specifically and markedly inhibits the growth of cancer cells with little cytotoxic effect on normal cells.

DMBO inhibits angiogenesis *in vitro*. Anti-angiogenic effects of DMBO were also examined using an *in vitro* model. DMBO selectively inhibited the formation of vascular

tubes on ECMatrix™ in a dose-dependent manner (Supplementary Fig. S6). The inhibition was 52 and 82% at 200 and 500 nM, respectively.

Effects of DMBO on the catalytic activity of heparanase. The expression of heparanase by tumor cells is closely related to its metastatic potential (34). To investigate the effects of DMBO on the catalytic activity of heparanase, biotinylated HS was incubated at 37 °C with recombinant human heparanase in the presence or absence of DMBO (59 to 236 μM). Strong inhibition was observed at 236 μM DMBO (Fig. 6A) and the inhibition was dose-dependent from 118 to 236 μM. However, the effect was less significant at 59 μM. An inhibitor for heparanase, suramin, prevented the catalytic activity of human heparanase at 70 μM (Fig. 6A).

Inhibition of heparan-degrading activity of LM8G7 by DMBO. During metastasis, the activation of a multitude of enzymes/proteins usually occurs. For example, the active secretion of heparanase or VEGF by tumor cells has been reported (10, 35). Hence, we determined the effects of DMBO on the heparan-degrading activity of LM8G7 cells. A high level of heparan-degrading activity was detected in LM8G7 cells. The control cell lysates without DMSO (positive control I) or with DMSO (positive control II) degraded the intact HS effectively (Fig. 6B). DMBO at 104 and 206 μM significantly inhibited the degradation of intact HS by 63 and 85%, respectively, but DMBO at 55 μM failed to inhibit the heparan-degrading activity (Fig. 6B). Thus, DMBO at higher concentrations significantly abolished the heparan-degrading activity of LM8G7 cells.

Effects of DMBO on the secretion of VEGF by LM8G7 cells. SPR analysis demonstrated that DMBO directly bound to VEGF (Fig. 1D). Hence, effects of DMBO on the secretion of VEGF by LM8G7 cells were studied. A significant amount of VEGF (0.42 ± 0.05 ng/ml) was detected in the control culture medium of LM8G7 cells, whereas exposure of the cells to DMBO inhibited the secretion of VEGF in a dose-dependent manner (Fig. 6C).

DMBO at 74, 148, and 295 μM effectively inhibited the secretion of VEGF by 18, 37, and 40%, respectively.

Discussion

The metastasis of cancer cells to specific sites in the body is mediated through a complex molecular process that involves multiple cell surface receptors, basement membrane components, intercellular adhesion molecules, and cytokines/growth factors (36). Once the molecules and their ligands involved in the pathways of cancer progression have been identified, it should be possible to develop synthetic compounds that inhibit these processes. Heparin and most of the HS mimetics that act to enhance the inhibition of inflammation and tumor metastasis are sulfated oligosaccharides (e.g., heparin derivatives, laminarin sulfate, and chitin derivatives) (37-39). It is difficult to develop and synthesize HS mimetic compounds, which perform multiple biological functions *in vivo* and *in vitro*. Low molecular weight HS mimetics with high specificity are rare. Among HS mimetics, PI-88 (phospho mannopentaose) has been reported as an antitumor agent, which significantly inhibits tumor growth, metastasis, and angiogenesis (40). An HS mimicking a pseudodisaccharide has been reported as an inhibitor of heparanase (41). All these compounds have a sugar-based structure. We herein report the synthesis and biological activities of a novel non-sugar-based compound, DMBO, which can mimic the pyranoside structure of sugar residues in HS.

We demonstrated here that DMBO strongly interacted with TNF-α, VEGF and HB-EGF directly as detected by SPR assay. The SPR signal of DMBO was significantly stronger than that of other structurally similar compounds having the same oxazine nucleus (Supplementary Fig. S3-S5). This indicates that the 2,6-difluorophenyl group of DMBO is important for the interaction with TNF-α, VEGF and HB-EGF. DMBO did not bind to other heparin-binding growth factors such as pleiotrophin and midkine (data not shown).

The biological activities of TNF-α have attracted much attention, and strategies developed for preventing the negative effects of TNF-α include neutralization of the cytokine using anti-TNF-α antibodies and the suppression of TNF-α synthesis. TNF-α activates key molecules involved in metastasis such as interleukin-8 (IL-8), an angiogenic Groa/KC chemokine, as well as matrix metalloproteinases and urokinase-plasminogen activators, both of which are involved in degradation of the ECM and cellular migration (42, 43). Recently, Murai et al. demonstrated the effects of a novel small molecule, SA13353 (1-[2-(1-adamantyl)ethyl]-1-pentyl-3-[3-(4-pyridyl)propyl]urea), as an active inhibitor of TNF-α production in animal models (44). DMBO also inhibited the binding of TNF-α to the anti-TNF-α antibody, and evidently inhibited the local production of TNF-α in an inflammatory model induced with TG and LPS in mice. Further, DMBO inhibited the proliferation of OVSAHO cells, which abundantly express TNF-α. These results support the effects of the direct binding of DMBO to TNF-α.

Moreover, DMBO completely inhibited the metastasis of LM8G7 cells to the liver at a low dose (0.5 mg/kg). Therefore, additional assays were carried out to confirm which biological steps of metastatic progression are affected by DMBO. Early tumor cell-platelet interactions and attachment to endothelial cells mediated by P-selectin binding are thought to be a critical move during hematogenous dissemination and escape from the immunological response (45), which correlate with metastatic progression. Fibronectin facilitates tumor cell adhesion to subendothelial matrices and extravasation from the microvasculature during hematogenous metastasis (46). In this study DMBO markedly inhibited the adhesion of LM8G7 cells to P-selectin and fibronectin. Thus, blocking of these interactions by a single injection of DMBO could reduce long-term establishment of metastatic nodules in the liver. The suppression of metastasis cannot be accounted solely by these processes. Additional mechanisms like inhibition of invasion and proliferation by DMBO are also likely to be

involved. Thus, DMBO appear to have multipotent effects on metastasis, the very first of which would be the inhibition of tumor cell attachment to platelets and endothelial cells. In addition, DMBO effectively inhibited angiogenesis *in vitro* in a concentration-dependent manner without affecting the proliferation of normal endothelial cells, suggesting that it is not toxic to normal cells.

Heparanase is known to be involved in the migration, invasion and proliferation of tumor cells (9). Moreover, DMBO blocked the catalytic activity of human heparanase at higher concentrations (104 and 206 μM). Therefore, DMBO may prevent the degradation of cell-surface and extracellular HS by heparanase. Supporting this assumption, the DMBO-exposed LM8G7 cells failed to degrade the biotinylated HS *in vitro*, indicating DMBO to have inhibited the secretion or the activity of heparanase.

Numerous studies have shown that overexpression of VEGF, a heparin-binding growth factor, and its receptor plays an important role in tumor-associated angiogenesis and subsequent growth and metastasis (47). Monoclonal antibodies to VEGF, notably bevacizumab (48), as well as small molecule inhibitors targeting the VEGFR kinases, such as sunitinib and sorafenib (49), have been reported to have anti-tumor activity. Many sugar-based derivatives have been reported as strong inhibitors of tumor progression and metastasis. However, evidence for the direct binding of small molecules to VEGF is still lacking. We herein demonstrated that DMBO bound directly to VEGF via non-covalent interactions. It was also found that DMBO at higher concentrations affected the secretion of VEGF by LM8G7 cells. Thus, the inhibition of heparanase along with inhibition of the migration, adhesion, invasion and proliferation of VEGF-positive LM8G7 cells is likely to be involved in the anti-tumor effects of DMBO.

The present study also demonstrated that DMBO, a non-sugar-based compound, completely inhibited the proliferation of SKOV-3 cells, which secrete HB-EGF, another protein essential for tumorigenesis. The SPR analysis showing the binding of DMBO

specifically to HB-EGF, supports this observation. Additional studies will be necessary to clarify the underlying mechanism. A result similar to this observation was reported for the diphtheria toxin (CRM197), which binds to HB-EGF and suppresses the growth of ovarian cancer cells (50).

Although we have synthesized many oxazine derivatives that bear the same nucleus as that of DMBO, to the best of our knowledge, this is the first report on a synthetic oxazine that mimics HS interacts directly with growth factors/cytokines, and has potential anti-metastatic activity. However, additional studies are needed to elucidate the mechanism of action of DMBO toward cancer cells.

Acknowledgements

Grant support: Japan Society for the Promotion of Science (K. S.) and Indian National Science Academy (K. S. R.).

References

1. Henriksson R, Grankvist K. Interactions between anticancer drugs and other clinically used pharmaceuticals: A review. Acta oncol 1989;28:451-62.
2. Weidmannt B, Abeles RH. Mechanism of inactivation of chymotrypsin by 5-butyl-3H-1,3-oxazine-2,6-dione. Biochemistry 1984;23:2373-76.
3. Kusakabe Y, Nagatsu J, Shibuya M, et al. Minimycin, a new antibiotic. J Antibiotics 1972;25:44-7.
4. Moorman AR, Abeles RH. New class of serine protease inactivators based on isatoic anhydride. J Am Chem Soc 1982;104:6785-6.
5. Mundhenke C, Meyer K, Drew S, et al. Heparan sulfate proteoglycans as regulators of fibroblast growth factor-2 receptor binding in breast carcinomas. Am J Pathol 2002;160:185-94.

6. Iozzo RV, San Antonio JD. Heparan sulfate proteoglycans: heavy hitters in the angiogenesis arena. J Clin Invest 2001;108:349-55.
7. Chu CL, Goerges AL, Nugent MA. Identification of common and specific growth factor binding sites in heparan sulfate proteoglycans. Biochemistry 2005;44:12203-13.
8. Vlodavsky I, Bar-Shavit R, Ishai-Michaeli R, et al. Extracellular sequestration and release of fibroblast growth factor: a regulatory mechanism?. Trends Biochem Sci 1991;16:268-71.
9. Vlodavsky I, Friedmann Y, Elkin M, et al. Mammalian heparanase: gene cloning, expression and function in tumor progression and metastasis. Nat Med 1999;5:793-802.
10. Goldshmidt O, Zcharia E, Abramovitch R, et al. Cell surface expression and secretion of heparanase markedly promote tumor angiogenesis and metastasis. Proc NatI Acad Sci USA 2002;99:10031-6.
11. Hulett MD, Freeman C, Hamdorf BJ, et al. Cloning of mammalian heparanase, an important enzyme in tumor invasion and metastasis. Nat Med 1999;5:803-9.
12. Sasisekharan R, Shriver Z, Venkataraman G, et al. Roles of heparan-sulphate glycosaminoglycans in cancer. Nat Rev Cancer 2002;2:521-28.
13. Ishida K, Wierzba MK, Teruya T, et al. Novel heparan sulfate mimetic compounds as antitumor agents. Chem Biol 2002;11:367-77.
14. Jayne DG, Perry SL, Morrison E, et al. Activated mesothelial cells produce heparin-binding growth factors: implications for tumour metastases. Br J Cancer 2000;82:1233-38.
15. Egberts JH, Cloosters V, Noack A, et al. Anti-tumor necrosis factor therapy inhibits pancreatic tumor growth and metastasis. Cancer Res 2008;68:1443-50.

16. Tammela T, Zarkada G, Wallgard E, et al. Blocking VEGFR-3 suppresses angiogenic sprouting and vascular network formation. Nature 2008;454:656-60.
17. Cohen T, Gitay-Goren H, Sharon R, et al. $VEGF_{121}$, a vascular endothelial growth factor (VEGF) isoform lacking heparin binding ability, requires cell-surface heparin sulfates for efficient binding to the VEGF receptors of human melanoma cells. J Biol Chem 1995;270:11322-6.
18. Miyamoto S, Hirata M, Yamanaki A, et al. Heparin-binding EGF-like growth factor is a promising target for ovarian cancer therapy. Cancer Res 2004;64:5720-7.
19. Ramnarain DB, Park S, Lee DY, et al. Differential gene expression analysis reveals generation of an autocrine loop by a mutant epidermal growth factor receptor in glioma cells. Cancer Res 2006;66:867-74.
20. Kim J, Jahng WJ, Vizio DD, et al. The phosphoinositide kinase PIKfyve mediates epidermal growth factor receptor trafficking to the nucleus. Cancer Res 2007;67:9229-37.
21. Miyamoto S, Yagi H, Yotsumoto F, et al. Heparin-binding epidermal growth factor-like growth factor as a novel targeting molecule for cancer therapy. Cancer Sci 2006;97:341-7.
22. Lee CM, Tanaka T, Murai T, et al. Novel chondroitin sulfate-binding cationic liposomes loaded with cisplatin efficiently suppress the local growth and liver metastasis of tumor cells in vivo. Cancer Res 2002;62:4282-8.
23. Fidler IJ, Nicolson GL. Organ selectivity for implantation survival and growth of B16 melanoma variant tumor lines. J Natl Cancer Inst 1976;57:1199-202.
24. Saito A, Kawai K, Takayama H, et al. Improvement of photoaffinity SPR imaging platform and determination of binding site of p62/SQSTM1 to p38 MAP kinase. Chem Asian J 2008;3:1607-12.

25. Pettipher ER, Labasi JM, Salter ED, et al. Regulation of tumour necrosis factor production by adrenal hormones in vivo: insights into the anti inflammatory activity of rolipram. Br J Pharmacol 1996;117:1530-4.

26. Weitz-Schmidt G, Gong KW, Wong CH, et al. Selectin/glycoconjugate binding assays for the identification and optimization of selectin antagonists. Anal Biochem 1999;273:81-8.

27. Karasawa K, Sugiura N, Hori Y, et al. Inhibition of experimental metastasis and cell adhesion of murine melanoma cells by chondroitin sulfate-derivatized lipid, a neoproteoglycan with anti-cell adhesion activity. Clin Exp Metastasis 1997;15:83-93.

28. Tanaka Y, Nakayamada S, Fujimoto H, et al. H-ras/mitogen-activated protein kinase pathway inhibits integrin-mediated adhesion and induces apoptosis in osteoblasts. J Biol Chem 2002;277:21446-52.

29. Xing JZ, Zhu L, Jackson JA, et al. Dynamic monitoring of cytotoxicity on microelectronic sensors. Chem Res Toxicol 2005;18:154-61.

30. Akalu A, Roth JM, Caunt M, et al. Inhibition of angiogenesis and tumor metastasis by targeting a matrix immobilized cryptic extracellular matrix epitope in laminin. Cancer Res 2007;67:4353-63.

31. Nakajima M, DeChavigny A, Johnson CE, et al. Suramin. A potent inhibitor of melanoma heparanase and invasion. J Biol Chem 1991;266:9661-6.

32. Takahashi H, Ebihara S, Okazaki T, et al. Clinical significance of heparanase activity in primary resected non-small cell lung cancer. Lung Cancer 2004;45:207-14.

33. Goyeneche AA, Caron RW, Telleria M. Mifepristone inhibits ovarian cancer cell growth *In vitro* and *In vivo*. Clin Cancer Res 2007;13:3370-9.

34. Koliopanos A, Friess H, Kleeff J, et al. Heparanase expression in primary and

metastatic pancreatic cancer. Cancer Res 2001;61:4655-9.

35. Asai T, Ueda T, Itoh K, et al. Establishment and characterization of a murine osteosarcoma cell line (LM8) with high metastatic potential to the lung. Int J Cancer 1998;76:418-22.
36. Bogenrieder T, Herlyn M. Axis of evil: molecular mechanisms of cancer metastasis. Oncogene 2003;22:6524–36.
37. Bar-Ner M, Eldor A, Wasserman L, et al. Inhibition of heparanase mediated degradation of extracellular matrix heparan sulfate by non-anticoagulant heparin species. Blood 1987;70:551-7.
38. Miao HQ, Elkin M, Aingorn E, et al. Inhibition of heparanase activity and tumor metastasis by laminarin sulfate and synthetic phosphorothioate oligodeoxynucleotides. Int J Cancer 1999;83:424-31.
39. Saiki I, Murata J, Nakajima M, et al. Inhibition by sulfated chitin derivatives of invasion through extracellular matrix and enzymatic degradation by metastatic melanoma cells. Cancer Res 1990;50:3631-7.
40. Ferro V, Dredge K, Liu L, et al. PI-88 and novel heparan sulfate mimetics inhibit angiogenesis. Semin Thromb Hemost 2007;33:557-68.
41. Takahashi S, Kuzuhara H, Nakajima M. Design and synthesis of a heparanase inhibitor with pseudodisaccharide structure. Tetrahedron 2001;57:6915-26.
42. Friedl P, Wolf K. Tumor-cell invasion and migration: diversity and escape mechanisms. Nat Rev Cancer 2003;3:362-74.
43. Esteve PO, Chicoine E, Robledo O, et al. Protein kinase C-zeta regulates transcription of the matrix metalloproteinase-9 gene induced by IL-1 and TNF-α in glioma cells via NF-kB. J Biol Chem 2002;277:35150-5.
44. Murai M, Tsuji F, Nose M, et al. SA13353 (1-[2-(1-Adamantyl)ethyl]-1-pentyl-3-

[3-(4-pyridyl)propyl] urea) inhibits TNF-α production through the activation of capsaicin-sensitive afferent neurons mediated via transient receptor potential vanilloid 1 in vivo. Eur J Pharmacol 2008;588:309-15.

45. Chen M, Geng JG. P-selectin mediates adhesion of leukocytes, platelets, and cancer cells in inflammation, thrombosis, and cancer growth and metastasis. Arch Immunol Ther Exp 2006;54:75-84.
46. Ruoslahti E. Fibronectin in cell adhesion and invasion. Cancer Metastasis Rev 1984;3:43-51.
47. Zhu Z, Witte L. Inhibition of tumor growth and metastasis by targeting tumor-associated angiogenesis with antagonists to the receptors of vascular endothelial growth factor. Invest New Drugs 1999;17:195-212.
48. Panares RL, Garcia AA. Bevacizumab in the management of solid tumors. Expert Rev Anticancer Ther 2007;7:433-45.
49. Grandinetti CA, Goldspiel BR. Sorafenib and sunitinib: novel targeted therapies for renal cell cancer. Pharmacotherapy 2007;27:1125-44.
50. Mitamura T, Higashiyama S, Taniguchi N, et al. Diphtheria toxin binds to the epidermal growth factor (EGF)-like domain of human heparin-binding EGF-like growth factor/diphtheria toxin receptor and inhibits specifically its mitogenic activity. J Biol Chem 1995;270:1015-9.

Figure Legends

Figure 1. Interaction between DMBO and growth factors/cytokines. A, Overview of the SPR analysis. DMBO (10 mM) was immobilized on the PGSs. Interactions were detected between DMBO and the growth factors/cytokines in solution by SPR imaging; B-D, the maximum SPR signal strength observed by DMBO and TNF-α (B), HB-EGF (C), or VEGF (D).

Figure 2. Effects of DMBO on the binding and secretion of TNF-α. A, Inhibitory effects of DMBO on the binding of TNF-α to anti-TNF-α antibody. Recombinant mouse TNF-α was incubated with the indicated concentrations of DMBO (15 to 148 μM). The bound TNF-α was quantified using the Quantikine Kit as outlined under Materials and Methods. % Inhibition of the binding of TNF-α to anti-TNF-α antibody against the concentration of DMBO is shown. Heparin (50 μg/ml) was used as a positive control. Data is represented as the mean ± SD for four replicates. B, Anti-inflammatory effects of DMBO on (TG + LPS)-induced inflammation in mice. Male C57BL/6 mice were injected intraperitoneally with 2 ml of 3% TG and LPS (1 μg) as described in Materials and Methods. Intravenous administration of DMBO (0.5, 1.5 or 5 mg/kg) and heparin (10 mg/kg) effectively suppressed the inflammation. The bar graph represents % inhibition of the infiltration of inflammatory cells into the peritoneal fluid by DMBO and heparin. C, Effects of DMBO (0.5, 1.5 or 5 mg/kg) and heparin (10 mg/kg) on the local production of TNF-α in the peritoneal cavities of the mice primed with TG and LPS. Data from the quantification of TNF-α are presented as the mean ± SD for three independent experiments and each experiment was conducted with 6 mice per group. * $P < 0.05$ and ** $P < 0.01$ versus control. *** $P < 0.005$ versus control.

Figure 3. Effects of DMBO against the metastatic potential of mouse osteosarcoma cells. C3H/HeN mice were intravenously injected with 1 x 10^6 LM8G7 cells in 200 μl of DMEM

via the tail. Some mice received an intravenous injection of DMBO (0.5, 1.0 or 1.5 mg/kg) suspended in 200 μL of DMEM 30 min prior to the injection of tumor cells. After 4 weeks, the mice were sacrificed, the number of liver nodules was counted macroscopically, and the liver weight was measured in the control and DMBO-injected animals. Representative livers from mice injected with LM8G7 cells treated with DMEM (A) and DMBO (0.5 mg/kg) (B) are shown. C, liver weight. Data represent mean values ± SD for three independent experiments and each experiment was conducted with 6 mice per group. * $P < 0.05$ versus control.

Figure 4. Effects of DMBO on the migration, adhesion and invasion of LM8G7 cells. A, Effects of DMBO on the migration of osteosarcoma cells. LM8G7 cells were grown to confluence in 6-well plates. The cell monolayers were wounded by scratching as described in Materials and Methods, and incubated with medium containing a vehicle, DMSO, or 0.2 μM of DMBO in DMSO. The phase-contrast images (x10 fields) of the wound healing process were photographed digitally with an inverted microscope at 0 h and after incubation of the cells at 37 °C for 24 h. B, The distance between the edges of the wound was measured, normalized to 100% at 0 h and presented. Data represent mean values ± SD for two independent experiments. C, Effects of DMBO on the adhesion of LM8G7 cells to P-selectin or fibronectin-coated plate. A P-selectin (open bars) or fibronectin (solid bars)-coated plate was incubated with DMBO (27 or 54 μM). LM8G7 (2×10^4) cells were seeded, and the adherent cells were determined after 1 h using Tetracolor One. Values obtained with control wells, which were not treated with DMBO, were taken as 100% cell adhesion. The % inhibition of the adhesion of LM8G7 cells by DMBO is presented. D, The % inhibition of the invasion of the LM8G7 cells by DMBO. Invasion across the Matrigel-coated porous membranes was determined in the presence or absence of DMBO (0.2 or 0.5 μM) as

described in Materials and Methods. The % inhibition of the invasion of LM8G7 cells by DMBO is presented. Data represent mean values ± S.D. for three determinations. * $P < 0.05$ versus control. ** $P < 0.01$ versus control.

Figure 5. Effects of DMBO on the viability and proliferation of normal and cancer cells. A, % Inhibition by DMBO of the proliferation of mouse endothelial cells. UV♀2 cells were cultured overnight and incubated with or without DMBO (195 μM) or mifepristone (155 μM, positive control) for an additional 48 h. TetraColor One (5 μL) was added to each well and the viable cells were quantified as described in Materials and Methods. B, % Inhibition of DMBO against the proliferation of ovarian cancer cells. SKOV-3 cells were cultured overnight and incubated with or without the indicated concentrations of DMBO (1, 17 or 195 μM) or mifepristone (155 μM). The total number of viable cells was determined as described above. Data represent the mean values ± S.D. for four identical wells from three independent experiments. * $P < 0.05$ versus control. ** $P < 0.01$ versus control. C, Real-time monitoring of the effects of DMBO on the proliferation of OVSAHO cells. OVSAHO cells were seeded in ACEA's 96X e-plate™ at a density of 15 x 10^3 cells per well, and continuously monitored using the RT-CES system up to 24 h, at which point DMBO (24 to 197 μM) was added. The cell index is plotted against the time. D, Real-time monitoring of the effects of DMBO on the proliferation of LM8G7 cells. LM8G7 cells were seeded in ACEA's 96X e-plate™ at a density of 5 x 10^3 cells per well and DMBO was added as described above. Data represent the mean values ± S.D. for three identical wells from three independent experiments.

Figure 6. The effects of DMBO on the catalytic activity of heparanse and the secretion of VEGF by LM8G7 cells. A, The % inhibition of rh-heparanase activity was plotted against the

concentration of DMBO. A heparan-degrading assay kit was used according to the manufacturer's directions. Briefly, 50 μL of biotinylated HS was incubated with 31 mIU of rh-heparanase in the presence or absence of serially diluted DMBO (59 to 236 μM). The effect of DMBO on the catalytic activity of rh-heparanase was determined as described in Materials and Methods. Suramin (70 μM) was used as a positive control. B, Mean absorbance of the intact HS remaining after the incubation of LM8G7 cell lysates in the presence or absence of DMBO is shown. The adhered LM8G7 cells were treated with DMBO at the indicated concentration (55, 104 or 206 μM). Using the cell lysates, the heparan-degrading activity was determined as described in Materials and Methods. The negative control (NC) contained the substrate but no cell lysate. PC I and PC II, positive controls I and II. C, Effect of DMBO on the secretion of VEGF by LM8G7 cells. LM8G7 cells were seeded into a 6-well plate and incubated overnight. After 24 h, the medium was replaced with a fresh serum-free medium containing 74, 148, or 295 μM of DMBO. The cells were further incubated for 48 h at 37 °C. The quantification of mouse VEGF in the cell supernatant was done using the Quantikine Immunoassay Kit as described in Materials and Methods. Data represent mean values ± SD for three independent experiments. * $P < 0.05$ versus control. ** $P < 0.01$ versus control.

Basappa et al.,

Figure 1

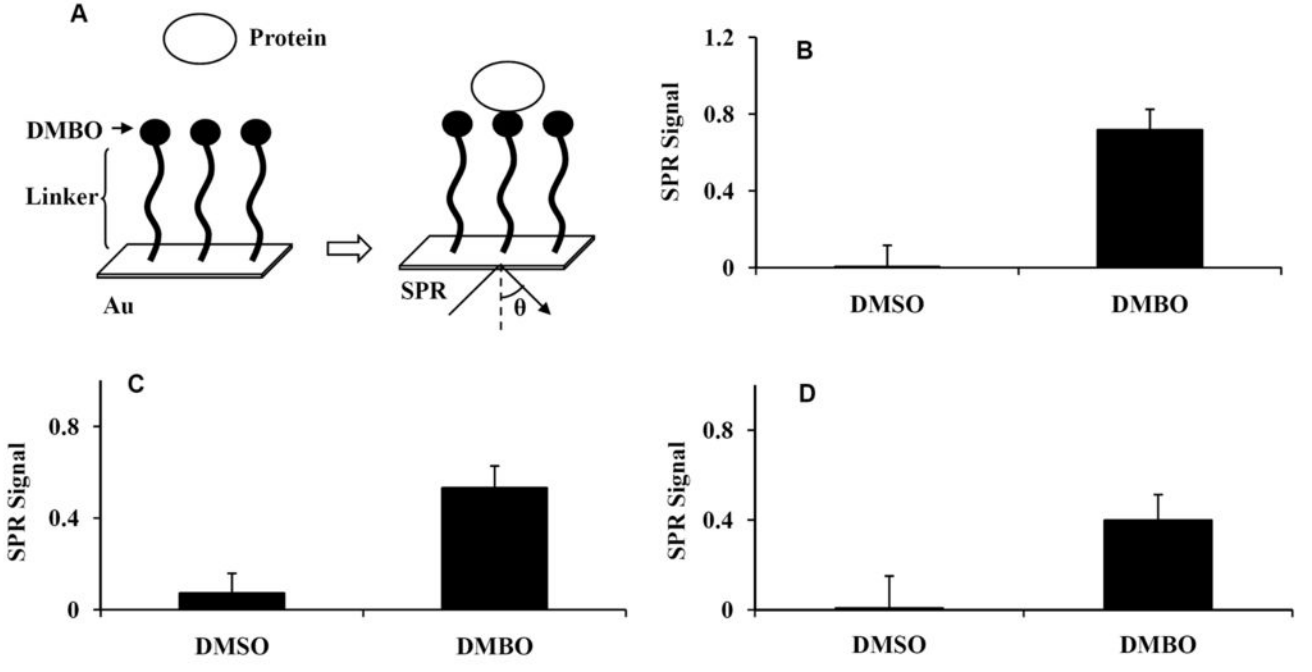

Figure 2

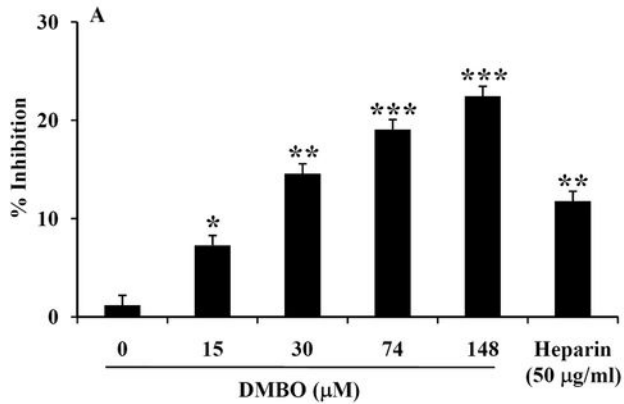
A
% Inhibition
30
20
10
0
*
**
***
***
**
0
15
30
74
148
Heparin
(50 µg/ml)
DMBO (µM)

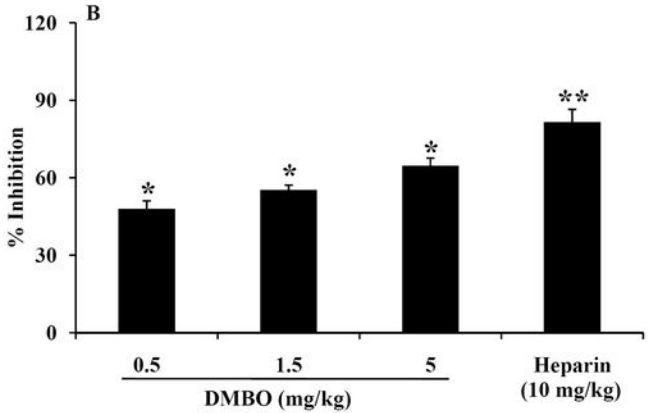
B
% Inhibition
120
90
60
30
0
*
*
*
**
0.5
1.5
5
Heparin
(10 mg/kg)
DMBO (mg/kg)

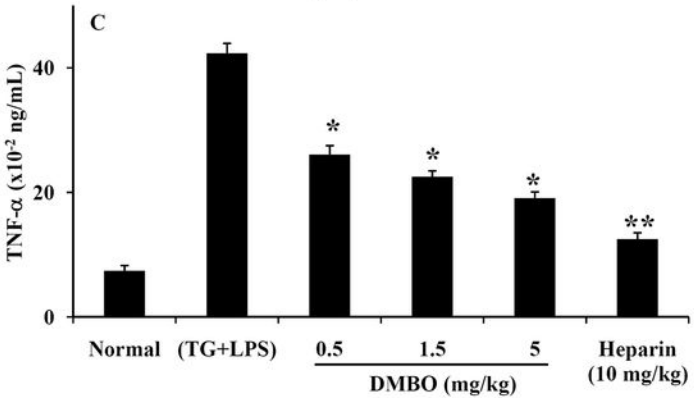
C
TNF-α (x10⁻² ng/mL)
40
20
0
*
*
*
**
Normal
(TG+LPS)
0.5
1.5
5
Heparin
(10 mg/kg)
DMBO (mg/kg)

Basappa et al.,

Figure 3

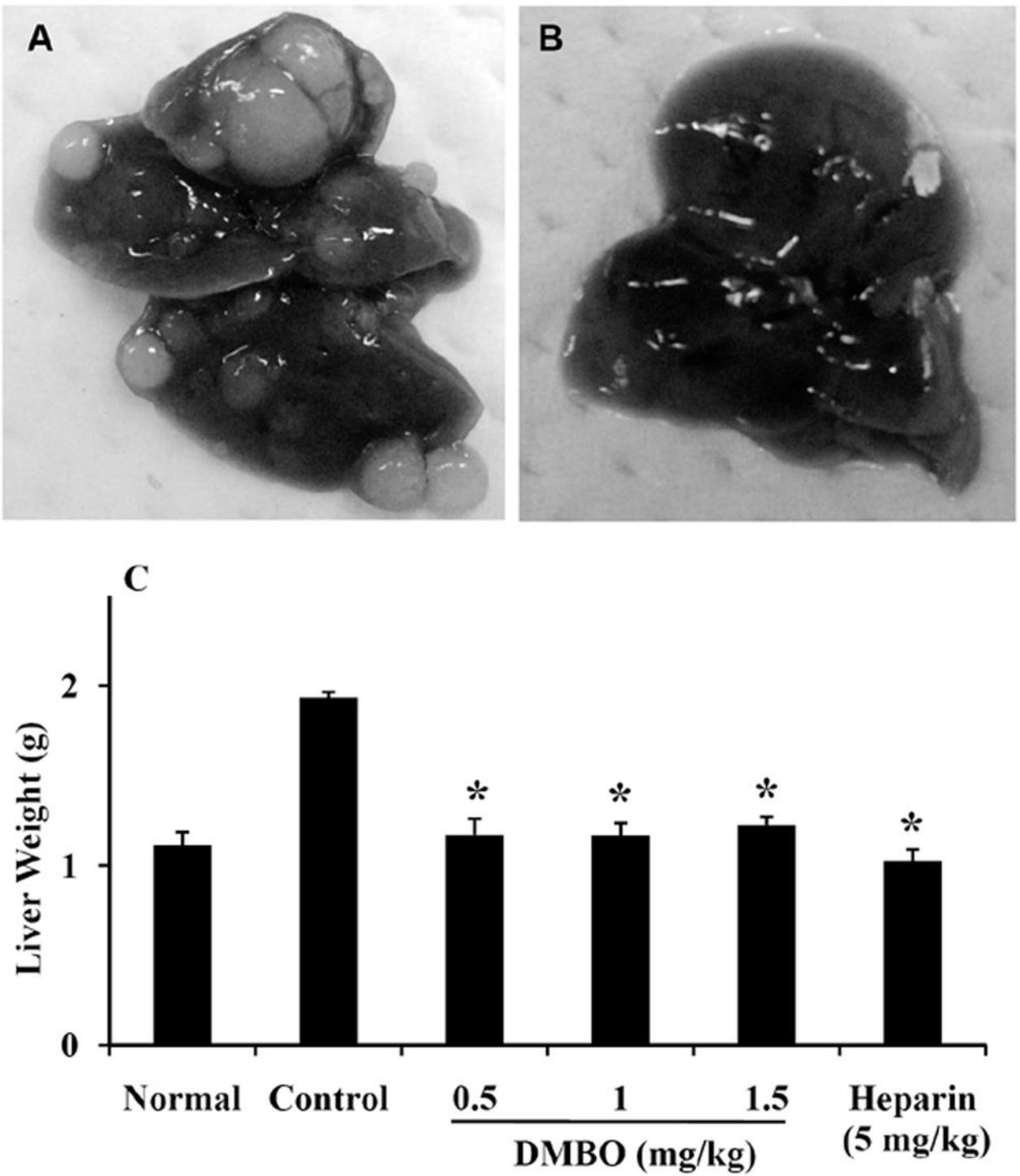

Figure 4

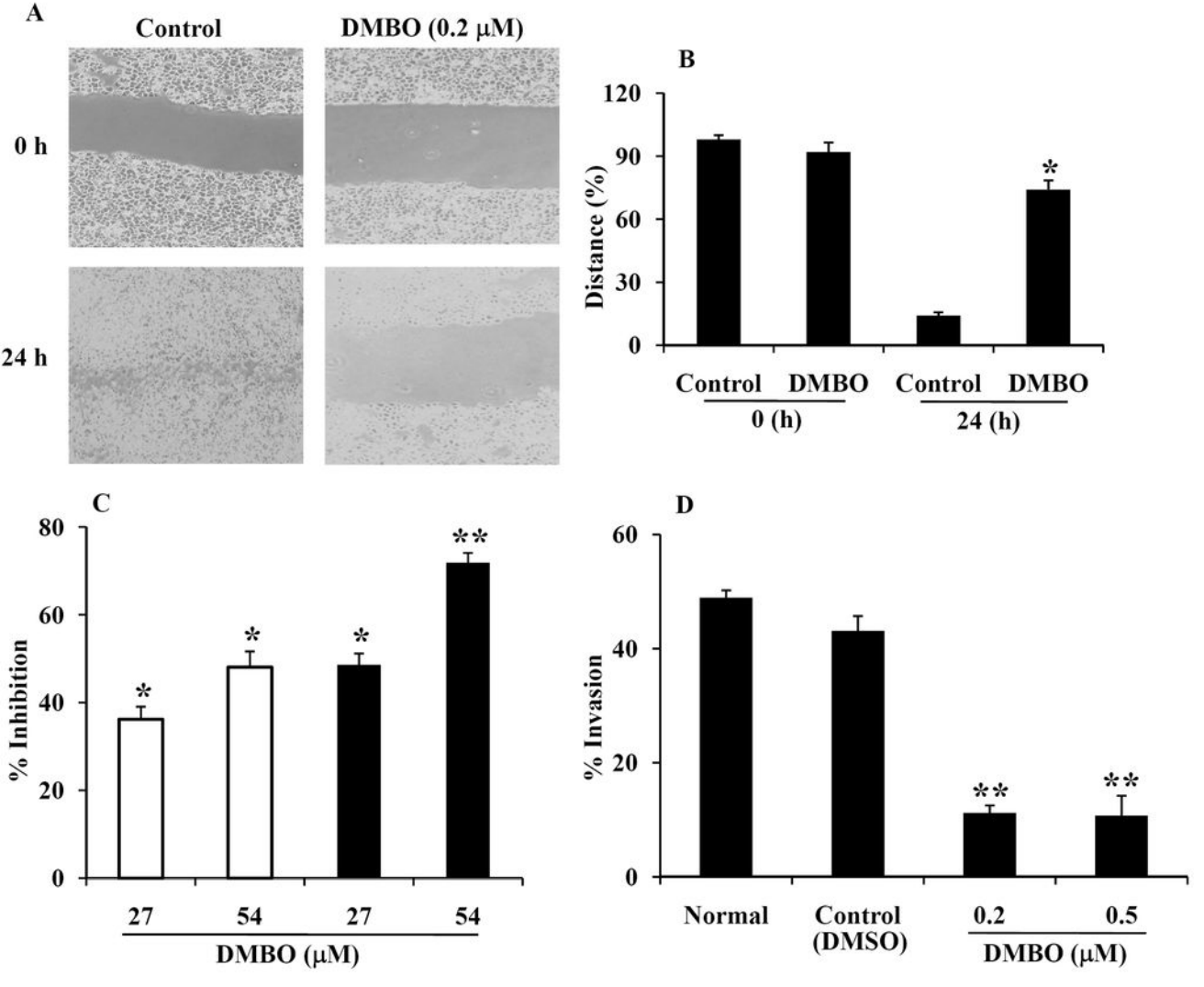
A
Control
DMBO (0.2 μM)
0 h
24 h
B
Distance (%)
120
90
60
30
0
*
Control
DMBO
Control
DMBO
0 (h)
24 (h)
C
% Inhibition
80
60
40
20
0
*
*
*
**
27
54
27
54
DMBO (μM)
D
% Invasion
60
40
20
0
**
**
Normal
Control (DMSO)
0.2
0.5
DMBO (μM)

Basappa et al.,

Figure 5

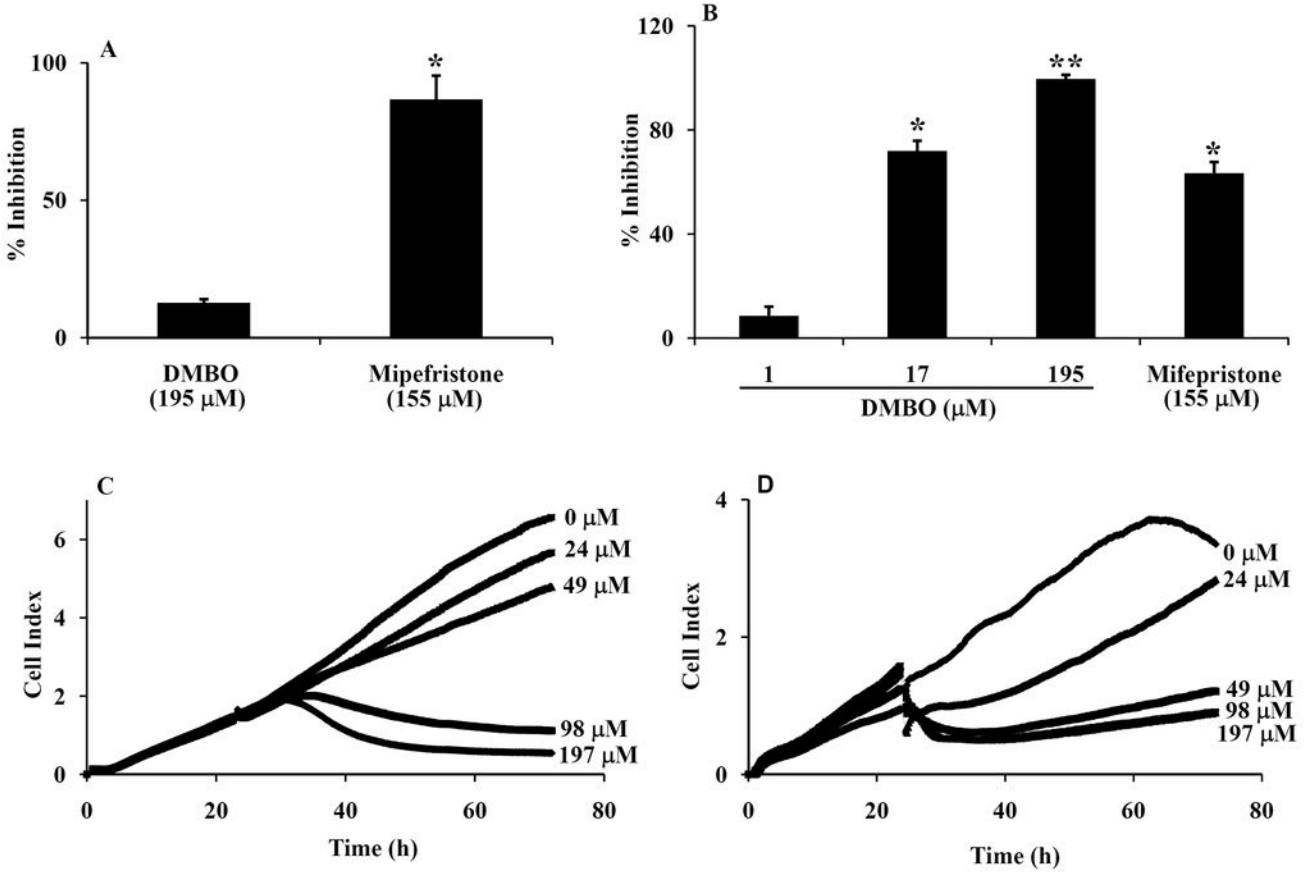

Basappa et al.,

Figure 6